

$0\nu\beta\beta$ decay to the first 2^+ state with a two-nucleon mechanism for a L - R symmetric modelDong-Liang Fang ^{1,2} and Amand Faessler³¹*Institute of Modern Physics, Chinese Academy of Science, Lanzhou 730000, China*²*School of Nuclear Science and Technology, University of Chinese Academy of Sciences, Beijing 100049, China*³*Institute for Theoretical Physics, Tübingen University, D-72076 Tübingen, Germany*

(Received 21 August 2022; accepted 3 January 2023; published 17 January 2023)

We develop the formalism for calculating the decay rate of neutrinoless double β decay to the 2^+ excited states within the L - R symmetric model. We consider the effects from induced hadronic currents up to next to leading order. The quasiparticle random phase approximation method in a spherical basis is adopted for the nuclear many-body calculation and the corresponding nuclear matrix elements are given. Also, the phase space factors are obtained with numerical electron wave functions. Our results suggest that the nuclear matrix elements are nucleus dependent and they are generally smaller than that of the decay to the ground states. And finally, we give a naive analysis of how current experiment data constrains the L - R symmetric model.

DOI: [10.1103/PhysRevC.107.015501](https://doi.org/10.1103/PhysRevC.107.015501)**I. INTRODUCTION**

New physics beyond the standard model is always the hottest topic in particle physics. Further, the origin of the neutrino mass could be one of the most important questions in this area. Perhaps, the most promising explanation for a small neutrino mass is the seesaw mechanism. The see-saw mechanism can usually be divided into different categories. To realize such mechanisms, different new physics models are proposed. One of the appealing proposals is the L - R symmetric model [1] with the underlying gauge symmetry $SU(2)_L \times SU(2)_R \times U(1)_{B-L}$. With two more Higgs particles introduced, one can naturally incorporate the seesaw mechanism into this model. There are different phenomenologies related to this model. One of the important consequences is the existence of the so-called neutrinoless double beta decay ($0\nu\beta\beta$ decay).

However, the underlying mechanism of $0\nu\beta\beta$ decay may not be unique. Thus, it is important to find a way to identify the decay mechanisms by future measurements. There are several proposals for this purpose, such as comparing the ratios of the decay rates for different candidates [2] or measuring the spectra and the angular correlations of the emitted electrons [3]. As an alternative, one also suggests to compare the decay rates of decays to ground and excited states [4], especially between the ground states and the 2^+ excited states [3].

In the minimal L - R symmetric model, for the decay to the ground state, due to the neutrino propagator's helicity suppression by the mass mechanism, the non-helicity-suppressed q term may play a dominant role [5]. Under such a scenario, the emission of P -wave electrons will surely lead to a visible effect on the angular correlation of the double β spectrum, this is investigated in [6]. Also, for another decay mode—neutrinoless double β decay to the 2^+ excited states [hereafter $0\nu\beta\beta(2^+)m$], contributions from such P -wave electrons will

become dominant. While different from the decay to ground states, the helicity suppressed m_e terms are negligible since these terms come from the next to leading order (NLO) parts of the hadronic current. So with such a physics model, we may probe the underlying mechanism by comparing these different decay modes. Unfortunately, $0\nu\beta\beta(2^+)$ is actually rarely investigated, and the only calculation available is done with the projected Hartree-Fock-Bogoliubov (pHFB) approach [7]. The pHFB calculation suggests that the decay is highly suppressed since the Nuclear Matrix Element (NME) is several orders of magnitude smaller than that of the decay to ground states (Hereafter $0\nu\beta\beta(0^+)$). This smallness is caused partly by the suppression from each part of the NME and partly by the cancellation among them. On the other hand, in [8], one finds that although the neutrino mass mechanism can contribute to this decay mode, their NME is about two orders of magnitude smaller than the q mechanism. These together make it impossible to observe $0\nu\beta\beta(2^+)$.

Nevertheless, our recent calculations [9] suggest that the NME in [7] is underestimated, our results are orders of magnitude larger than those of [7] and cancellations among different components are not observed especially for $M_{\eta'}$. These results may suggest that decay to the first 2^+ states is not that heavily suppressed as previously expected. In all previous calculations, only the vector and axial-vector parts of the hadronic current are considered. Another important component, namely, the pseudoscalar part from the pion pole [10], is not taken into account. As suggested in [11], this pseudoscalar piece is accounted as a LO contribution like the vector and axial-vector parts. In most $0\nu\beta\beta$ calculations, the NLO weak-magnetism contribution is also taken into account. In this work, we incorporate all these parts into the calculation and study their effects on the NME's.

The calculation of NME relies on various nuclear many-body approaches, and we limit our discussions to traditional

ones with effective nuclear forces, leaving out those of *ab initio* methods using a nuclear force starting from the bare nucleon-nucleon interaction. For the decay to the ground states with the standard neutrino mass mechanism, several calculations have been done over the decades. First we mention the time-consuming large scale shell model (LSSM) calculations [12,13], which take advantage of the existence of the shell gap, and separates the particles of the core and the nucleons of the valence part.

Apart from LSSM calculations, which are applicable to limited cases due to the large computation requirement, several other methods can be applied to more occasions, e.g., the IBM-2 method [14], the DFT methods of nonrelativistic [15] and relativistic versions [16], the project HFB method [17], as well as the quasiparticle random phase approximation (QRPA) method [18–21], which takes intermediate states into account. For recent reviews of these calculations, we refer to [22,23].

Meanwhile, the NME calculations for the nonstandard LR-symmetric model with the inclusion of the non-helicity-suppressed q terms are less frequently considered for $0\nu\beta\beta(0^+)$. Recent calculations have been done by QRPA [6,24,25], LSSM [26–30] as well as by pHFB [31]. Especially for [26–28,32], contributions from standard model (SM) effective field theory have been thoroughly analyzed besides the LR-symmetric model. There are also other calculations starting from SM effective field theories which have different expressions as traditional LR symmetric models [11,33].

Compared to the above calculations of decay to the ground states, the decay to the excited 2^+ state is rarely discussed, and the most recent calculations are from about two decades ago [8] as mentioned above. To investigate this special decay mode, we adopt the QRPA method with realistic nuclear forces [9]. Our previous results suggest that the final NMEs are larger than expected with only the vector and axial vector parts of the hadronic currents included. In this work, we include more components up to NLO to make a more thorough investigation.

This article is arranged as follows. At first we present the formalism we use. It is followed by the results for the phase space factors and the nuclear matrix elements. Then we discuss constraints on the L - R model parameters from current results. Finally we give a conclusion as well as an outlook.

II. FORMALISM

In the L - R symmetric models, such as $SU(2)_L \times SU(2)_R \times U(1)_{B-L}$, after two successive spontaneous symmetry breakings, the left- and right- handed gauge bosons acquire masses through the Higgs mechanism, and in general the left- and right-handed gauge bosons are mixed [1,5]:

$$\begin{pmatrix} W_L \\ W_R \end{pmatrix} = \begin{pmatrix} \cos \xi & -\sin \xi \\ \sin \xi & \cos \xi \end{pmatrix} \begin{pmatrix} W_1 \\ W_2 \end{pmatrix}. \quad (1)$$

Here, ξ is the mixing angle and W_1, W_2 the mass eigenstates of W bosons.

The neutrinos acquire masses through their Yukawa coupling with Higgs bosons [1]:

$$\begin{pmatrix} \nu_L \\ N_R \end{pmatrix} = \begin{pmatrix} U & U' \\ V' & V \end{pmatrix} \begin{pmatrix} \nu_M \\ N_M \end{pmatrix}, \quad (2)$$

where $\nu_L^T = (\nu_e, \nu_\mu, \nu_\tau)$ and $N_R^T = (N_e, N_\mu, N_\tau)$ are the three flavor left- and right-handed neutrinos. ν_M and N_M are their light and heavy mass eigenstates. The seesaw mechanism can be naturally fulfilled in this model [1].

Starting from the left- and right-gauge-fermion interactions, the effective weak Hamiltonian can be written following the definition in [5]:

$$H_{\text{eff}} = \sqrt{\frac{1}{2}} G_F \cos \theta_C (j_{L\mu} \tilde{J}_L^\mu + j_{R\mu} \tilde{J}_R^\mu) + \text{H.c.}, \quad (3)$$

where the lepton currents are

$$j_{L(R)}^\mu(\vec{x}) = \bar{\psi}_e(\vec{x}) \gamma^\mu P_{L(R)} \psi_\nu(\vec{x}) \quad (4)$$

with $P_L = (1 - \gamma_5)/2$ and $P_R = (1 + \gamma_5)/2$, respectively.

In the current model, the hadronic currents have the form

$$\begin{aligned} \tilde{J}_{L\mu} &\approx J_{L\mu}, \\ \tilde{J}_{R\mu} &\approx \eta J_{L\mu} + \lambda J_{R\mu}. \end{aligned} \quad (5)$$

Here,

$$\eta \equiv -(g_R/g_L) \tan \xi [1 - (M_1/M_2)^2] / [1 + \tan^2 \xi (M_1/M_2)^2], \quad (6)$$

$$\lambda \equiv (g_R/g_L)^2 [(M_1/M_2)^2 + \tan^2 \xi] / [1 + \tan^2 \xi (M_1/M_2)^2]. \quad (7)$$

Here, M_1 and M_2 are the mass eigenvalues of W_1 and W_2 gauge bosons, respectively.

Within the nonrelativistic impulse approximation, under the Breit frame, the left- or right-handed hadronic currents have the form

$$\begin{aligned} J_{L\mu}(\vec{x}) &= (J_0(\vec{x}), \vec{J}_L(\vec{x})), \\ J_{R\mu}(\vec{x}) &= (J_0(\vec{x}), \vec{J}_R(\vec{x})), \end{aligned} \quad (8)$$

where

$$\begin{aligned} J_0(\vec{x}) &= \sum_{n=1}^A g_V(q^2) \delta(\vec{x} - \vec{r}_n), \\ \vec{J}_L &= \sum_{n=1}^A -[g_A(q^2) \vec{\sigma}_n - g_P(q^2) (\vec{\sigma}_n \vec{q}) \vec{q} \\ &\quad + i \frac{g_M(q^2)}{2m_p} (\vec{\sigma}_n \times \vec{q})] \delta(\vec{x} - \vec{r}_n), \\ \vec{J}_R &= \sum_{n=1}^A [g_A(q^2) \vec{\sigma}_n - g_P(q^2) (\vec{\sigma}_n \vec{q}) \vec{q} \\ &\quad - i \frac{g_M(q^2)}{2m_p} (\vec{\sigma}_n \times \vec{q})] \delta(\vec{x} - \vec{r}_n). \end{aligned} \quad (9)$$

According to angular momentum conservation, for $0\nu\beta\beta(2^+)$, the emitted electrons must be coupled to total angular momentum $J = 2$, this suggests that the dominant

TABLE I. The decomposition coefficients of NMEs for M_λ , M_η , and M'_η . Here, $g_A = g_A(0)$.

i	1	2	3	4	5	6	7
$C_{\lambda i}$	$\frac{1}{3}g_A^2$	$-\frac{2}{3}g_A^2$	$\sqrt{\frac{7}{3}}g_A^2$	1	$-\sqrt{\frac{3}{2}}g_A$		
$C_{\eta i}$	$\frac{1}{3}g_A^2$	$-\frac{2}{3}g_A^2$	$\sqrt{\frac{7}{3}}g_A^2$	-1	0		
$C'_{\eta i}$						$\sqrt{\frac{1}{2}}g_A$	$-\sqrt{\frac{3}{2}}g_A$

contribution comes from the combination of decomposed partial waves $s_{1/2} - p_{3/2}$ [5]. Substituting the hadronic currents into the S matrix, the decay width can then be written as [5,7]

$$\Gamma = G_1 |M_\lambda(\lambda) - M_\eta(\eta)|^2 + G_2 |M'_\eta(\eta)|^2. \quad (10)$$

Here, G 's are phase space factors and M 's are the NMEs. $\langle\lambda\rangle$ and $\langle\eta\rangle$ are new physics parameters connected to λ and η defined above as [6] $\langle\eta\rangle = \eta |\sum_j U_{ej} V_{ej}^*|$ and $\langle\lambda\rangle = \lambda |\sum_j U_{ej} V_{ej}^* (g'_V/g_V)|$. Here, g_V and g'_V are the vector coupling constants for left- and right-handed currents, respectively. U and V are neutrino mass mixing matrix elements. And j sums over the light neutrino mass eigenstates.

The phase space factor (PSF) can be expressed as [7]

$$G_i = \frac{4\pi}{\ln 2R_n^4} \int dE_1 dE_2 \frac{(G \cos \theta_C)^4}{32\pi^6} f_i p_1 p_2 E_1 E_2 \times \delta(E_1 + E_2 - 2m_e - Q_{\beta\beta}(2^+)). \quad (11)$$

Here,

$$f_1 = 3[|f^{-2-1}|^2 + |f_{21}|^2 + |f^{-1-2}|^2 + |f_{12}|^2],$$

$$f_2 = 3[|f^{-2-1}|^2 + |f^{-1-2}|^2 + |f^{-2-1}|^2 + |f^{-1-2}|^2]. \quad (12)$$

$$h_1(q, r) = \frac{1}{g_A^2(0)} j_1(qr) \left[g_A^2(q^2) + 2 \frac{g_A(q^2)g_P(q^2)q^2}{2m_p} - \frac{g_P^2(q^2)q^4}{(2m_p)^2} - 2 \frac{g_M^2(q^2)q^2}{(2m_p)^2} \right],$$

$$h_2(q, r) = \frac{1}{g_A^2(0)} j_1(qr) \left[g_A^2(q^2) - \frac{g_A(q^2)g_P(q^2)q^2}{2m_p} + \frac{1}{5} \frac{g_P^2(q^2)q^4}{(2m_p)^2} + \frac{1}{5} \frac{g_M^2(q^2)q^2}{(2m_p)^2} \right],$$

$$h_3(q, r) = \frac{1}{g_A^2(0)} \left\{ j_1(qr) \left[g_A^2(q^2) - \frac{g_P(q^2)g_A(q^2)q^2}{2m_p} + \frac{1}{5} \frac{g_P^2(q^2)q^4}{(2m_p)^2} + \frac{1}{5} \frac{g_M^2(q^2)q^2}{(2m_p)^2} \right] - j_3(qr) \left[\frac{3}{35} \frac{g_P^2(q^2)q^4}{(2m_p)^2} + \frac{3}{35} \frac{g_M^2(q^2)q^2}{(2m_p)^2} \right] \right\},$$

$$h'_3(q, r) = \frac{1}{g_A^2(0)} j_3(qr) \left[\sqrt{\frac{3}{5}} \frac{g_P^2(q^2)q^4}{(2m_p)^2} + \sqrt{\frac{3}{5}} \frac{g_M^2(q^2)q^2}{(2m_p)^2} \right],$$

$$h_4(q, r) = \frac{g_V^2(q^2)}{g_V^2(0)} j_1(qr), \quad h_5(q, r) = \frac{g_V(q^2)g_A(q^2)}{g_V(0)g_A(0)} j_1(qr), \quad h_6(q, r) = h_7(q, r) = \frac{g_V(q^2)g_A(q^2)}{g_A^2(0)} \frac{r_+ j_1(qr)}{r}. \quad (14)$$

Here, $q = |\vec{q}|$ is the exchange momentum carried by the neutrino propagator. The $g_\alpha(q^2)$'s are the form factors. It can be written in an empiric dipole form in general: $g_V(q^2) = g_V(0)/(1 + q^2/\Lambda_V)^2$ and $g_A(q^2) = g_A(0)/(1 + q^2/\Lambda_A)^2$. Here, $g_V(0) = 1$ and $g_A(0) = 1.27$, and

For these f functions such as f_{12} , we follow the convention in [34]. In our definition, the phase space factor are with the unit of y^{-1} , this is obtained by dividing R_n^2 to Eq. (11) of [7]. Here $R_n = 1.2A^{1/3}$ fm is the conventionally defined nuclear radius. By deriving this, the no finite de Broglie wave length correction (no FBWC) approximation is used [5].

The expressions for the NME are much more complicated, and we follow the conventions in [7], divide the NME into seven parts:

$$M_\lambda = \sum_{i=1}^5 C_{\lambda i} M_i,$$

$$M_\eta = \sum_{i=1}^5 C_{\eta i} M_i,$$

$$M'_\eta = \sum_{i=6}^7 C'_{\eta i} M_i.$$

For the coefficients C 's, we follow the definition of [7] as well and they are tabulated in Table I, where we have absorbed g_A into the NME unlike the conventional treatment where coupling constants g 's are included in PSFs.

The NME can be further expressed as $M_i = \langle 2_f^+ || \mathcal{M}_i || 0_i^+ \rangle$, and these operators \mathcal{M}_i can be expressed in a general form:

$$\mathcal{M}_i = \frac{2R_n}{\pi} \int \frac{qdq}{q + E_N} h_i(q, r) \mathcal{O}_i. \quad (13)$$

Here, $E_N = E_{mx} + M_m - (M_i + M_f + E_{2^+})/2$ is the intermediate state excitation energy relative to the initial and final states. And h is usually called the neutrino potential and \mathcal{O} is the angular transition operator.

Where, for different NME components, the detailed forms for neutrino potential h_i is as follows:

we take $\Lambda_V = 0.85$ GeV and $\Lambda_A = 1.1$ GeV for the energy cutoff. In the nuclear environment, $g_A(0)$ is usually quenched with a not definitely known origin. Therefore in the current work we adopt two values for this coupling constant: The bare one and a quenched one with a quenching factor

TABLE II. PSFs for various nuclei from the current work and that of [5] as well as current experimental limits. For results from [5], we have converted to our convention. We also present the constraints on new physics parameter on two special cases.

	Q (MeV)	G_1 (10^{-15} y^{-1})		G_2 (10^{-15} y^{-1})		$t_{1/2}^{\text{limit}}(\text{y})$	$ \lambda \gg \eta , m_{\beta\beta}$		$ \eta \gg \lambda , m_{\beta\beta}$	
		this work	[5]	this work	[5]		2 ⁺	0 ⁺ [6]	2 ⁺	0 ⁺ [6]
⁷⁶ Ge	1.480	6.86	7.37	4.77	5.12	$>2.1 \times 10^{24}$ [38]	$<2.13 \times 10^{-5}$	$<5.07 \times 10^{-7}$	$<4.56 \times 10^{-6}$	$<2.81 \times 10^{-9}$
⁸² Se	2.219	50.12	55.28	40.11	44.30	$>1.0 \times 10^{22}$ [39]	$<8.35 \times 10^{-5}$		$<5.63 \times 10^{-5}$	
⁹⁶ Zr	2.572	140.4		117.2		$>9.1 \times 10^{20}$ [39]	$<2.76 \times 10^{-3}$		$<2.38 \times 10^{-4}$	
¹⁰⁰ Mo	2.495	134.2	149.8	111.3	124.3	$>1.6 \times 10^{23}$ [39]	$<2.52 \times 10^{-4}$		$<1.73 \times 10^{-5}$	
¹¹⁶ Cd	1.520	18.18		12.98		$>6.2 \times 10^{22}$ [39]	$<1.75 \times 10^{-4}$		$<2.32 \times 10^{-5}$	
¹²⁸ Te	0.423	0.225	0.267	0.0825	0.0985					
¹³⁰ Te	1.991	76.41	91.37	60.04	71.84	$>1.4 \times 10^{23}$ [39]	$<2.35 \times 10^{-5}$		$<5.11 \times 10^{-6}$	
¹³⁶ Xe	1.639	35.61	44.99	26.33	33.42	$>2.6 \times 10^{25}$ [39]	$<2.43 \times 10^{-6}$	$<4.35 \times 10^{-7}$	$<4.17 \times 10^{-6}$	$<2.12 \times 10^{-9}$

$g_A = 0.75g_{A0}$. And $g_M(q^2) = (1 + \kappa_1)g_V(q^2)$ [18] with $\kappa_1 = \mu_p - \mu_n$. Also $g_P(q^2) = 2m_p g_A(q^2)/(q^2 + m_\pi^2)$ is given by the Partially Conserved Axial Currents (PCAC) hypothesis.

And the angular operators \mathcal{O} s have the forms

$$\begin{aligned}
\mathcal{O}_1 &= \vec{\sigma}_1 \cdot \vec{\sigma}_2 [\hat{r} \otimes \hat{r}]^{(2)}, \\
\mathcal{O}_2 &= [\vec{\sigma}_1 \otimes \vec{\sigma}_2]^{(2)}, \\
\mathcal{O}_3 &= [[\vec{\sigma}_1 \otimes \vec{\sigma}_2]^{(2)} \otimes [\hat{r} \otimes \hat{r}]^{(2)}]^{(2)}, \\
\mathcal{O}'_3 &= [[\vec{\sigma}_1 \otimes \vec{\sigma}_2]^{(2)} \otimes [[\hat{r} \otimes \hat{r}]^{(2)} \otimes [\hat{r} \otimes \hat{r}]^{(2)}]^{(4)}]^{(2)}, \\
\mathcal{O}_4 &= [\hat{r} \otimes \hat{r}]^{(2)}, \\
\mathcal{O}_5 &= [(\vec{\sigma}_1 + \vec{\sigma}_2) \otimes [\hat{r} \otimes \hat{r}]^{(2)}]^{(2)} \quad (15)
\end{aligned}$$

for the nonprimed NMEs M_λ and M_η .

And

$$\begin{aligned}
\mathcal{O}_6 &= [(\vec{\sigma}_1 - \vec{\sigma}_2) \otimes [\hat{r} \otimes \hat{r}_+]^{(1)}]^{(2)}, \\
\mathcal{O}_7 &= [(\vec{\sigma}_1 - \vec{\sigma}_2) \otimes [\hat{r} \otimes \hat{r}_+]^{(2)}]^{(2)} \quad (16)
\end{aligned}$$

for the primed NME M'_η .

Compared to the expression in [7], M_3 has one extra term induced by the hadronic current, we denote it by M'_3 . For M_4 – M_7 , no corrections from the induced hadronic current are presented.

For the sake of comparison with the decay to the ground state cases, we find that we have also AA , AP , PP , and MM components for the space-space current-current interactions (M_1 , M_2 , and M_3) coming from different components of induced hadronic current. Except for M_1 , one finds that PP and MM components are suppressed by a factor smaller than 1/5 compared to AA and AP components.

The NMEs are calculated in our case with the nuclear many-body approach, the so-called pn -QRPA as well as charge conserving QRPA methods both with realistic nuclear forces [9]. The detailed expression can be found in [9]

$$\begin{aligned}
M_i &= \sum_{pp'n'}^{J^\pi m} \langle 2^+_{f'} | [c_p^\dagger \tilde{c}_n]_{J'} | | J^\pi m_f \rangle \langle J^\pi m_f | | J^\pi m_f \rangle \\
&\quad \times \langle J^\pi m_i | [c_p^\dagger \tilde{c}_n]_J | | 0^+_i \rangle. \quad (17)
\end{aligned}$$

The expressions for the one-body densities as well as the overlap of the initial and final intermediate states can also be

found in [36], where the final 2⁺ states are obtained by charge conserving QRPA [35,36].

III. RESULTS AND DISCUSSIONS

A. Phase space factors

For the calculation of PSFs, we use the numerical package RADIAL [37] for the electron wave functions and we follow the convention in [34]. We use a uniform charge distribution for the calculations of the nuclear static charge potential and we choose the charge radius to be the same as the nuclear radius. We neglect the screening effect from the orbital electrons since it gives minor corrections to PSF [34] in the case of the decay to the ground state.

The results of PSFs of various nuclei are presented in Table II, we also list these nuclei's Q values. For most nuclei except ¹²⁸Te, PSFs span a range of about two orders of magnitude. Three nuclei have Q values larger than 2 MeV, and of which ⁹⁶Zr has the largest PSF for the decay into the excited state. ¹⁰⁰Mo has almost the same values for the PSF as ⁹⁶Zr, since their Q values are close. While ⁸²Se has a larger Q value, its PSFs are somehow smaller than those of ¹³⁰Te mostly due to its smaller atomic number Z .

We also present results from an earlier calculation [5], where a Taylor expansion of the electron wave function is used. For ⁷⁶Ge, we have also results from [7], $G_1 = 7.34 \times 10^{-15} \text{ y}^{-1}$ and $G_2 = 5.10 \times 10^{-15} \text{ y}^{-1}$, which are basically the same as the results in [5] with a deviation less than 1% since they use a similar treatment for electron wave functions. Our current numerical results generally agree with their results quantitatively. We find the deviations for ours and theirs are about 10%–30%, the current numerical results are smaller than their predictions. There is a strong trend of an increase for the deviations as Z increases. This is reasonable, with the growth of Z the nuclear radius R also increases. Since the conventional Taylor expansion method uses αZ and WR as variables, the errors will grow with the increase of these variables. One finds the largest phase space factor for ¹⁰⁰Mo from their calculations. If this nucleus has also the largest NME, then it can be one of the most promising candidates for a future experimental search. To explore such a possibility, we need high precision nuclear many-body calculations. We will proceed into this direction in the next part.

TABLE III. NMEs for decay to 2^+ with $g_A = g_{A0} = 1.27$. Here, a and b refer to two different cases with AV-18 and CD-Bonn short range correlations adopted.

		^{76}Ge		^{82}Se		^{96}Zr		^{100}Mo		^{116}Cd		^{128}Te		^{130}Te		^{136}Xe	
		a	b	a	b	a	b	a	b	a	b	a	b	a	b	a	b
M_1	AA	0.641	0.640	0.790	0.789	0.027	0.027	0.205	0.205	0.198	0.199	0.700	0.700	0.643	0.643	0.334	0.333
	AP	0.481	0.480	0.649	0.648	0.046	0.046	0.141	0.141	-0.058	-0.057	0.425	0.425	0.449	0.448	0.563	0.562
	PP	-0.087	-0.087	-0.149	-0.149	-0.022	-0.022	-0.022	-0.022	0.067	0.067	-0.044	-0.043	-0.070	-0.070	-0.206	-0.206
	MM	-0.033	-0.033	-0.098	-0.098	-0.027	-0.028	-0.007	-0.007	0.071	0.072	0.018	0.018	-0.016	-0.016	-0.182	-0.183
	tot.	1.001	1.000	1.193	1.191	0.024	0.023	0.317	0.317	0.279	0.280	1.099	1.100	1.006	1.006	0.510	0.506
M_2	AA	-0.249	-0.252	-0.005	-0.006	0.238	0.239	-0.052	-0.054	-0.992	-0.996	-0.268	-0.269	-0.175	-0.175	0.405	0.408
	AP	0.207	0.210	-0.028	-0.027	-0.229	-0.230	0.265	0.267	0.564	0.568	0.142	0.143	0.059	0.060	-0.416	-0.419
	PP	-0.034	-0.034	-0.002	-0.003	0.029	0.030	-0.043	-0.043	-0.066	-0.067	-0.022	-0.022	-0.012	-0.012	0.044	0.045
	MM	-0.021	-0.023	-0.005	-0.006	0.014	0.014	-0.022	-0.023	-0.035	-0.037	-0.014	-0.015	-0.008	-0.009	0.022	0.023
	tot.	-0.097	-0.098	-0.041	-0.042	0.052	0.052	0.148	0.147	-0.530	-0.532	-0.162	-0.163	-0.136	-0.136	0.056	0.058
M_3	AA	-0.049	-0.049	0.118	0.118	-0.008	-0.008	0.158	0.158	0.015	0.015	-0.098	-0.098	-0.009	-0.009	0.407	0.407
	AP	-0.031	-0.031	-0.059	-0.059	-0.005	-0.005	-0.034	-0.034	-0.053	-0.053	-0.039	-0.039	-0.044	-0.044	-0.056	-0.056
	PP	0.004	0.004	-0.000	-0.000	-0.001	-0.001	-0.001	-0.001	0.001	0.001	0.006	0.006	0.003	0.003	-0.009	-0.009
	MM	0.001	0.001	-0.003	-0.003	-0.001	-0.001	-0.002	-0.002	-0.002	-0.002	-0.001	-0.001	-0.001	-0.001	-0.005	-0.005
	tot.	-0.074	-0.074	0.056	0.056	-0.015	-0.015	0.121	0.121	-0.040	-0.040	-0.132	-0.132	-0.052	-0.052	0.336	0.336
M'_3	PP	-0.003	-0.003	-0.023	-0.023	0.004	0.004	-0.021	-0.021	-0.012	-0.012	-0.019	-0.019	-0.019	-0.019	-0.019	-0.019
	MM	-0.001	-0.001	-0.012	-0.012	0.001	0.001	-0.010	-0.010	-0.007	-0.007	-0.010	-0.010	-0.010	-0.010	-0.009	-0.009
	tot.	-0.004	-0.004	-0.035	-0.035	0.005	0.005	-0.031	-0.031	-0.019	-0.019	-0.029	-0.029	-0.030	-0.030	-0.028	-0.028
M_4		-0.147	-0.147	-0.123	-0.123	-0.072	-0.071	0.121	0.120	0.142	0.142	-0.188	-0.188	-0.139	-0.139	0.119	0.119
M_5		-0.061	-0.061	-0.216	-0.216	-0.257	-0.257	0.045	0.045	-0.124	-0.124	-0.130	-0.130	-0.161	-0.161	-0.280	-0.280
M_λ		0.398	0.399	0.952	0.952	0.262	0.261	0.284	0.285	0.909	0.911	0.384	0.385	0.597	0.597	1.527	1.523
M_η		0.597	0.598	0.862	0.862	0.005	0.004	0.112	0.114	0.431	0.435	0.558	0.559	0.626	0.626	0.854	0.849
M_6		0.631	0.640	0.314	0.315	0.128	0.128	0.481	0.484	-0.609	-0.615	0.803	0.816	0.669	0.679	0.054	0.049
M_7		-1.241	-1.251	-0.336	-0.339	0.419	0.422	-0.080	-0.083	0.948	0.951	-1.752	-1.762	-1.346	-1.353	0.187	0.190
M'_η		2.496	2.520	0.804	0.810	-0.537	-0.542	0.557	0.564	-2.021	-2.032	3.446	3.474	2.694	2.715	-0.242	-0.251

B. Nuclear matrix elements

While PSF can be fairly well determined with decent accuracy within about several percent, the NME's have larger uncertainties, greater than a factor of two [22]. In the current work we adopt a QRPA for the many-body calculations. Compared to the LSSM approach, QRPA has the advantage of a small computation requirement with the price of less accuracy.

For the QRPA method with realistic forces several renormalization parameters are needed to reproduce experimental data. We fit the pairing parameters by the experimental pairing gaps. And we renormalize the residual forces by $g_{pp}^{T=1}$ to eliminate $M_F^{2\nu}$ and $g_{pp}^{T=0}$ to reproduce the measured $2\nu\beta\beta$ NME.

All our results for the NME's are presented in Tables III and IV. The two tables correspond to two possible values of the axial vector coupling constant g_A commonly used in the literature. In these tables we also give the results with two different short range correlations (src's) marked as a and b for AV-18 and CD-Bonn [40], respectively, and we find these different src's barely change the results. As we are aware, different choices of src's will change the NME's for $0\nu\beta\beta(0^+)$ by about 5–10%. Therefore, $0\nu\beta\beta(2^+)$ is less sensitive to the choice of the src's. This suggests that the two nucleons involved in this decay are farther away from each other, as we shall see in a quantitative analysis later.

As shown in Eq. (14), except for M_1 , the PP and MM terms are suppressed by a factor of about 1/5–1/10. Therefore, since all the terms related to spherical Bessel function j_3 in M_3 are contained in PP and MM terms, they are heavily suppressed. Even though not suppressed by this small factor, the MM terms are generally smaller for M_1 . On the contrary, for most cases, the AP term plays an important role and they are supposed to be the LO contribution [11].

We first discuss the bare g_A case. For M_1 , besides the LO AA contribution, the major correction of about 2/3 comes from AP term as mentioned above. For most nuclei, this term leads to an enhancement for the final results but for ^{116}Cd , it gives a 30% reduction. For ^{136}Xe , it gives the largest contribution, even larger than AA , this makes it the dominant term in M_1 for this nucleus. Meanwhile for most nuclei, the PP term gives the reductions from 10%–20% relative to the AA term. Two exceptions are the ^{116}Cd and ^{136}Xe cases: for the former, this term gives an enhancement about 30% relative to the AA term which nearly cancels the reduction from the AP term as we discussed above; for the latter, PP gives a 2/3 reduction relative to AA , this term and the AP term together gives nearly the same contribution as AA . The MM terms are supposed to be NLO contributions [11]. For M_1 , it gives negligible contributions for the nuclei ^{100}Mo , ^{128}Te , and ^{130}Te , while corrections for the other nuclei ranges from 5% to 50%.

TABLE IV. The same as Table III but with $g_A = 0.75g_{A0}$.

	⁷⁶ Ge		⁸² Se		⁹⁶ Zr		¹⁰⁰ Mo		¹¹⁶ Cd		¹²⁸ Te		¹³⁰ Te		¹³⁶ Xe		
	<i>a</i>	<i>b</i>	<i>a</i>	<i>b</i>	<i>a</i>	<i>b</i>	<i>a</i>	<i>b</i>	<i>a</i>	<i>b</i>	<i>a</i>	<i>b</i>	<i>a</i>	<i>b</i>	<i>a</i>	<i>b</i>	
<i>M</i> ₁	AA	0.634	0.634	0.786	0.785	0.027	0.027	0.193	0.193	0.200	0.200	0.699	0.698	0.644	0.644	0.333	0.332
	AP	0.476	0.476	0.648	0.647	0.045	0.045	0.137	0.137	-0.058	-0.057	0.424	0.424	0.448	0.447	0.563	0.561
	PP	-0.086	-0.086	-0.149	-0.149	-0.022	-0.022	-0.022	-0.022	0.067	0.067	-0.043	-0.043	-0.070	-0.070	-0.206	-0.205
	MM	-0.033	-0.033	-0.098	-0.098	-0.027	-0.028	-0.007	-0.006	0.071	0.072	0.018	0.019	-0.016	-0.015	-0.181	-0.183
	tot.	0.991	0.991	1.187	1.185	0.022	0.022	0.302	0.302	0.280	0.281	1.097	1.098	1.007	1.006	0.508	0.505
<i>M</i> ₂	AA	-0.237	-0.240	-0.005	-0.006	0.240	0.241	-0.119	-0.121	-0.962	-0.966	-0.272	-0.273	-0.172	-0.173	0.404	0.407
	AP	0.204	0.207	-0.027	-0.025	-0.226	-0.227	0.277	0.279	0.553	0.558	0.144	0.145	0.059	0.060	-0.414	-0.418
	PP	-0.033	-0.034	-0.003	-0.003	0.029	0.029	-0.043	-0.044	-0.066	-0.066	-0.022	-0.023	-0.012	-0.012	0.044	0.045
	MM	-0.021	-0.022	-0.005	-0.006	0.013	0.014	-0.022	-0.023	-0.035	-0.037	-0.014	-0.015	-0.008	-0.009	0.022	0.023
	tot.	-0.087	-0.089	-0.039	-0.040	0.056	0.057	0.092	0.091	-0.509	-0.511	-0.165	-0.165	-0.134	-0.134	0.056	0.058
<i>M</i> ₃	AA	-0.049	-0.049	0.118	0.118	-0.007	-0.007	0.149	0.149	0.018	0.018	-0.099	-0.100	-0.010	-0.010	0.407	0.406
	AP	-0.031	-0.031	-0.059	-0.058	-0.005	-0.005	-0.034	-0.034	-0.054	-0.054	-0.039	-0.038	-0.044	-0.044	-0.056	-0.056
	PP	0.004	0.004	-0.000	-0.000	-0.001	-0.001	-0.001	-0.001	0.001	0.001	0.006	0.006	0.003	0.003	-0.009	-0.009
	MM	0.001	0.001	-0.003	-0.003	-0.001	-0.001	-0.002	-0.002	-0.002	-0.002	-0.001	-0.001	-0.001	-0.001	-0.005	-0.005
	tot.	-0.074	-0.074	0.056	0.056	-0.014	-0.014	0.112	0.112	-0.038	-0.038	-0.133	-0.133	-0.053	-0.053	0.336	0.336
<i>M</i> ' ₃	PP	-0.003	-0.003	-0.023	-0.023	0.004	0.004	-0.021	-0.021	-0.013	-0.012	-0.019	-0.019	-0.019	-0.019	-0.019	-0.019
	MM	-0.001	-0.001	-0.012	-0.012	0.001	0.001	-0.010	-0.010	-0.007	-0.007	-0.010	-0.010	-0.010	-0.010	-0.009	-0.009
	tot.	-0.004	-0.004	-0.035	-0.035	0.005	0.005	-0.031	-0.031	-0.020	-0.020	-0.029	-0.029	-0.030	-0.030	-0.028	-0.028
<i>M</i> ₄		-0.146	-0.146	-0.123	-0.122	-0.071	-0.071	0.120	0.120	0.143	0.143	-0.187	-0.188	-0.140	-0.140	0.119	0.119
<i>M</i> ₅		-0.061	-0.062	-0.214	-0.214	-0.258	-0.257	0.048	0.048	-0.124	-0.124	-0.128	-0.128	-0.161	-0.161	-0.280	-0.279
<i>M</i> _λ		0.161	0.162	0.489	0.489	0.194	0.193	0.170	0.171	0.568	0.569	0.133	0.133	0.280	0.280	0.943	0.941
<i>M</i> _η		0.391	0.392	0.535	0.535	0.032	0.031	0.027	0.028	0.170	0.172	0.395	0.395	0.411	0.411	0.427	0.425
<i>M</i> ₆		0.632	0.641	0.312	0.312	0.128	0.127	0.479	0.482	-0.612	-0.618	0.799	0.813	0.671	0.681	0.052	0.047
<i>M</i> ₇		-1.242	-1.252	-0.333	-0.336	0.422	0.424	-0.094	-0.097	0.948	0.952	-1.748	-1.758	-1.347	-1.355	0.187	0.190
<i>M</i> ' _η		1.874	1.893	0.598	0.602	-0.406	-0.410	0.432	0.437	-1.518	-1.526	2.577	2.598	2.024	2.040	-0.183	-0.190

For the extreme case of ⁹⁶Zr, the *MM* term has an equal size to *AA* due to the smallness of the latter.

For ⁹⁶Zr, *M*₁ is heavily suppressed, it is one order of magnitude smaller than other nuclei, and a careful check suggests that this smallness comes from the cancellation from different intermediate states, this differs from the case of ⁷⁶Ge, where different intermediate states add up together (see Fig. 1 of [9]). For all other nuclei, the total *M*₁ is generally within one order of magnitude, e.g., for ⁷⁶Ge, ⁸²Se, ¹²⁸Te, and ¹³⁰Te, its value is around 1.

The case for *M*₂ is quite different from *M*₁. For the *AA* component, different nuclei differ by several orders of magnitude, especially for ⁸²Se, it is heavily suppressed by the cancellations from different intermediate states. This cancellation also reduces the NME for ¹⁰⁰Mo. For other nuclei it has a value of about 0.2–0.3, but for the two cases with semimagic nuclei involved in the transition process, the results are somehow enhanced. Further investigation is needed for the possible relation between the magicity and this enhancement.

The correction from the pseudoscalar current is much more pronounced for *M*₂. For *M*₁ the *AP* term is about one order of magnitude larger than the *PP* term. Unlike for *M*₁, *AP* terms here mostly appear for cancellations, this causes an overall smallness of *M*₂ for most nuclei compared to *M*₁. The semimagic nuclei—as already mentioned above—have generally large *AA* terms, however for ¹³⁶Xe, the *AP* term exactly cancels the *AA* term. This leads to a suppressed *M*₂;

meanwhile for ¹¹⁶Cd, the cancellation from *AP* is smaller compared to *AA*. Thus we have the largest *M*₂ for this nucleus. As for ¹³⁶Xe, a nearly exact cancellation between *AA* and *AP* terms also happens for ⁷⁶Ge and ⁹⁶Zr. For ¹⁰⁰Mo, we find that the contribution from *AP* is about 5 times larger than that from *AA*. While for Te isotopes, *AP* reduces the results by about 50%. The *PP* term behaves like NLO contributions by the suppression from a small coefficient, their contributions are generally within a magnitude of 10%. So does the NLO *MM* term which contributes with about 10% for most cases.

Thus for most nuclei, *M*₂ is around 0.1 due to the cancellations between *AA* and *AP* terms, with the exception of ⁸²Se where all the components are small. ¹¹⁶Cd is the one with the largest *M*₂ about 0.5. As a result, our calculations suggest that *M*₂ is generally one order of magnitude smaller than *M*₁.

For most nuclei, *M*₃ is generally smaller than *M*₁ but similar to *M*₂. However, unlike the smallness caused by the cancellation between *AA* and *AP* terms for *M*₂, the magnitude of each component of *M*₃ is generally much smaller than the counterparts in *M*₁ or *M*₂. For ¹⁰⁰Mo and ¹³⁶Xe, the situation is a bit different: *AA* terms for them are close to that of *M*₁, but on the other hand, there is no large enhancement from the *AP* term for *M*₃, therefore those *M*₃ are generally smaller. And we find that for *M*₃, *PP* and *MM* terms are negligible. In general, except ¹³⁶Xe, *M*₃'s are around or smaller than 0.1.

We also find that the induced M'_3 is much smaller and barely gives visible contributions. But for ^{82}Se and ^{130}Te , M'_3 is comparable to M_3 , and gives a cancellation for the former nucleus and an enhancement for the latter.

In general, for the space-space components of hadronic currents, the inclusion of pseudoscalar and weak-magnetism terms, especially the AP term, will change the NME drastically and these changes are usually not negligible. Whether these contributions are positive or negative is nucleus dependent.

M_4 comes from the time-time component of hadronic currents and the induced current will not contribute to this component. As in [9], they are generally with the magnitude of 0.1 and the difference for different nuclei are generally within a factor of two. The largest value is found for ^{128}Te and the smallest from ^{96}Zr , differed nearly by a factor of 3.

M_5 is the space-time component of hadronic currents. Their values are generally close to M_4 with a magnitude around 1, but differ in details, such as the phases. The relative magnitude of these two NME's is nucleus dependent.

M_λ and M_η are induced from the coupling of \vec{q} and the relative coordinate of the two decaying nucleons \vec{r} . The difference between M_λ and M_η comes from the space-time and time-time components of the nuclear currents, it can be defined as $\delta M = 2M_4 - \sqrt{3}/2g_A M_5$. This suggests that for nuclei with M_4 and M_5 close to each other, such as ^{82}Se or ^{130}Te , this difference is small. On the other hand, this difference is also related to g_A . For all nuclei in our calculation, M_λ and M_η are with the same phase, this means they will cancel or add up to each other depending on the relative sign of $\langle\eta\rangle$ and $\langle\lambda\rangle$. For ^{76}Ge , ^{82}Se , ^{128}Te , and ^{130}Te , M_λ is smaller than M_η , while for other nuclei, M_λ is larger. In general, except for ^{136}Xe , M_λ and M_η are about one order of magnitude smaller than $M_{0\nu}(0^+)$ (to compare our results with those in various literatures, we need to divide the current results by g_{A0}^2). ^{136}Xe does have M_λ larger than 1 in our convention, but it is still less than half of the values for $M_{0\nu}(0^+)$.

M'_η are actually induced by the coupling of the \vec{q} term in the neutrino propagator and the center of mass (c.m.) coordinate of the two decaying nucleons \vec{r}_+ . The differences of M_6 and M_7 originate from the coupled angular momenta of the c.m. and relative coordinates, and thus are closely related to the orbitals of the decaying nucleons. In our calculation, we find for most nuclei, these two terms give coherent contribution but for ^{96}Zr and ^{136}Xe , they cancel each other leading to suppressed M'_η 's. For most nuclei, we have also larger M_7 , but for ^{96}Zr , M_7 is suppressed and is much smaller than M_6 . Also in most cases, M'_η is much larger than M_λ and M_η . Instead of one order of magnitude smaller than corresponding $M^{0\nu}(0^+)$, they are generally smaller within a factor of one-half. This differs with previous studies [7] where these NMEs are supposed to be several orders of magnitude smaller than $M^{0\nu}(0^+)$ and hence can be safely neglected. We will study the consequence of this dominance for the role of determining new physics parameters in the following section.

As presented in Table III, different src's produce actually negligibly smaller deviations like for the light neutrino mass mechanism of $0\nu\beta\beta(0^+)$. On the other hand, a comparison

of Tables III and IV suggests that quenching of g_A affects the final results drastically. In QRPA calculations the quenching affects the final results twofold:

- (1) First we fit our model parameter $g_{pp}^{T=0}$ by the $2\nu\beta\beta$ NME which is related to g_A . Therefore, quenching of g_A will affect the choice of this parameter and subsequently the individual NMEs.
- (2) Second the quenching changes the coefficients C 's in Table I which are then multiplied with the individual partial NME's to get the final total NME's.

For the current calculation, we find that the change of the parameter $g_{pp}^{T=0}$ induced by quenching will not largely change the individual NMEs, their changes are within 10%. Hence, the change of the final results can be directly connected to the quenched value of g_A in the coefficients C .

For M_λ , only the coefficients of M_4 are independent of g_A , and all other coefficients have a dependence linear or squared on g_A . Therefore, the quenching generally reduces M_λ by a magnitude from 30% to 50% for different nuclei. The largest reduction in percentage is found for ^{128}Te , where the NME for the quenched case is only one-third of that of the bare g_A case. The reduction for M_η is similar to that of M_λ , we now have no g_A linear dependent terms any more. The general reduction is from 30% to 70%, the largest reduction is found for ^{100}Mo with more than 70%. While for ^{96}Zr an enhancement is observed, but for this nucleus, all the individual NME's are small and they cancel each other significantly, the presence of quenching largely reduces the cancellation of M_1-M_3 to M_4 which then leads to the enhancement. All these behaviors for various nuclei stem from the interplay between M_4 and other individual NME's which are reduced by g_A . Drastic reductions are also found for M'_η with a nearly fixed factor $q = g_A/g_{A0}$ since the two terms are both proportional to g_A and the $g_{pp}^{T=0}$ dependence is weak for M_6 and M_7 . Therefore, as for the decay to the ground states, the role of g_A is important. We need to understand the origin of the quenching and the precise value of g_A for the $\beta\beta$ decay, we also need to determine whether the quenching is operator dependent.

C. Constraints on L - R symmetric model

Unlike for the decay to the ground state, where the neutrino mass mechanism is supposed to be dominant, the neutrino mass mechanism for $0\nu\beta\beta(2^+)$ can only be triggered by nuclear recoil [8] and hence is suppressed by a factor of $Q/2M$ compared to the $\langle\lambda\rangle$ and $\langle\eta\rangle$ terms. In [8], an estimation suggests that their NMEs are about several orders of magnitude smaller than that of the LR mechanism. Since this NME for the mass mechanism in the decay to excited state is extremely hindered, we do not expect to be able to observe this decay mode with the dominance of the mass mechanism.

Therefore measurements of $0\nu\beta\beta(2^+)$ can be used as perfect constraints on new physics parameters such as $\langle\lambda\rangle$ or $\langle\eta\rangle$. In this section, with the calculated NME and PSF as well as the experimental limit presented in Table II, we perform a simple analysis on several extreme cases. Currently the most stringent constraint for half-lives is that of ^{136}Xe ,

which pushes the limit to 10^{25} y while others are two or three orders of magnitude shorter. For ^{96}Zr , the lower limit is 10^{20} y, which is much shorter than all others. While [6] provides a way of probing different mechanisms from comparisons of different nuclei, the current method would help distinguish the underlying new physics within one isotope. This is done by comparing the decay rates to the ground and excited states as we shall show.

1. $|\lambda| \gg |\eta|$

In the λ dominant case (see Table II), Eq. (10) becomes $\Gamma = G_1 M_\lambda^2 |\langle \lambda \rangle|^2$ and the most stringent constraints for λ are obtained from ^{136}Xe . With our calculated NME's, we obtain the constraint $|\lambda| < 2.43 \times 10^{-5}$. Other nuclei yield generally the same magnitude except ^{96}Zr and ^{100}Mo which set limits one order of magnitude larger. Since all these nuclei except ^{136}Xe have basically similar M_λ , these larger limits generally are due to shorter half-life limits. In Table II, we present constraints obtained in [6] from decay to ground states for two nuclei from QRPA calculations without considering the hadronic induced currents. With a later calculation [25], one finds that the NME for $0\nu\beta\beta(0^+)$ is slightly enhanced, but this will not change the general magnitude of the constraints. Therefore, we can make a direct comparison. Our results suggest that for the λ dominant case, the constraints for ^{76}Ge differs by two orders of magnitude while for ^{136}Xe this difference is less than one order of magnitude while comparing our results with those from [6]. The half-life lower limits used for $0\nu\beta\beta(0^+)$ for both nuclei are around 10^{25} y, while for $0\nu\beta\beta(2^+)$, ^{76}Ge has a half-life lower limit one order of magnitude shorter. However, ^{136}Xe has the similar half-life lower limits to the 2^+ and ground states. Combining these results, we find that for certain nuclei (^{136}Xe here), for the case of λ dominance, the half-lives for the two modes are within a difference of two orders of magnitude, this could perhaps be used in the future for the identification of the decay mechanism if both modes are observed.

2. $|\lambda| \ll |\eta|$

For this case, Eq. (10) becomes $\Gamma = (G_1 M_\eta^2 + G_2 M_\eta^2) |\langle \eta \rangle|^2$ and the most stringent constraints come also from ^{136}Xe . However, ^{76}Ge and ^{130}Te yield also constraints close to ^{136}Xe . They all require that $|\eta|$ is smaller than about 10^{-6} . However, these constraints are far looser than those of $0\nu\beta\beta(0^+)$, where a limit around $|\eta| < 10^{-9}$ is obtained assuming the dominance of the η mechanism. If this case is true in nature, it will not be possible to observe the 2^+ decay in these nuclei, since we have a suppression for about 6 orders of magnitude for $0\nu\beta\beta(2^+)$ compared to $0\nu\beta\beta(0^+)$ for ^{136}Xe and 4–5 orders of magnitude for other nuclei. If future measurements do push the half-life limit of $0\nu\beta\beta(2^+)$ to 4–5 orders of magnitude longer, we can then rule out for both λ and η mechanisms.

3. $|\lambda| \sim |\eta|$

More general cases are presented in Fig. 1. For these cases, since $\langle \eta \rangle$ and $\langle \lambda \rangle$ share the same phase $e^{i\psi}$, Eq. (10)

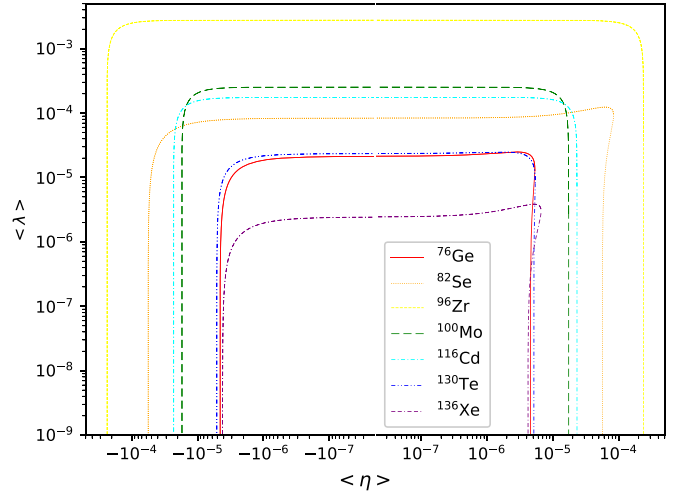


FIG. 1. Constraints on $\langle \lambda \rangle$ and $\langle \eta \rangle$ from $0\nu\beta\beta(2^+)$ decay. The region outside the curves is excluded by the current limits obtained from the measurements and our calculations.

can be written explicitly as $\Gamma = G_1 M_\lambda^2 |\langle \lambda \rangle|^2 + (G_1 M_\eta^2 + G_2 M_\eta^2) |\langle \eta \rangle|^2 - 2G_1 M_\lambda M_\eta \langle \lambda \rangle \langle \eta \rangle$. In the current convention, λ is always positive and the sign for η is not definite. Since different nuclei give constraints of λ and η on different orders of magnitude, we use a logarithm scale in the graph. The interference term of η and λ rotates the long axis of the ellipse to the first quadrant. From the figure, we can clearly see that, like in the λ or η dominant cases, ^{136}Xe sets the most stringent constraints. While ^{76}Ge and ^{130}Te set both less tight constraints for λ and η . And it is obvious that the future slight improvement of the measurement will surely set more stringent constraints for these two nuclei. This is highly probable for ^{130}Te , of which the current half-life lower limit is about two orders of magnitude smaller than that for ^{136}Xe . Better half-life lower limits for other nuclei will also improve our analysis. A combined analysis with decay to ground states could give us more hints on the relative magnitude of $\langle \eta \rangle$ and $\langle \lambda \rangle$.

In general, the measurement of decay to the 2^+ excited states offers a way for the discrimination of the underlying mechanism. For example, for ^{136}Xe , within our calculations, a half-time lower limit for about 2 orders of magnitude longer than the observed half-life of $0\nu\beta\beta(0^+)$ will rule out the possibility of the existence of the λ mechanism dominance. However, these conclusions rely heavily on the NME calculations, and need further verifications from other many-body calculations.

IV. CONCLUSIONS AND OUTLOOKS

In this work, we systematically investigate the decay rates of $0\nu\beta\beta(2^+)$ under the L - R symmetric model, where both the λ and η mechanisms are involved. We incorporate the contributions from induced currents and find that the pseudoscalar current is important for NME calculations. Our results suggest that the NME is nucleus dependent and may differ by up to one order of magnitude, also the NME for the two

different mechanisms in the same nucleus can be differed by more than one order of magnitude. We also improve the phase space factor calculations by using numerical electron wave functions. These results lead to different constraints on different nuclei both from different NME's and different current lower limits of decay half-lives. With the comparison to 0 $\nu\beta\beta$ (0⁺), we can constrain the underlying mechanisms within an individual nucleus. These comparisons suggest that for the special λ dominant case, ¹³⁶Xe has the potential for comparable decay half-lives for decays to both the ground state and 2⁺ excited state. Future experiments could shift the lower limit up and set more stringent constraints on the new physics parameters for another nucleus, and even have the potential of discovering the possible existence of right-handed gauge bosons. Meanwhile, to draw a more solid conclusion,

more nuclear many-body calculations are needed to make a better prediction of the NMEs which are keys for these investigations.

ACKNOWLEDGMENTS

This work is supported by the National Key Research and Development Program of China (2021YFA1601300). This work is also supported by the “Light of West China” and “From Zero to One” programs from CAS and Guangdong Major Project of Basic as well as Applied Basic Research No. 2020B0301030008 from Guangdong Province. The numerical calculations in this paper have been carried out on the supercomputing system in the Southern Nuclear Science Computing Center.

-
- [1] R. N. Mohapatra and G. Senjanovic, *Phys. Rev. D* **23**, 165 (1981).
- [2] E. Lisi, A. M. Rotunno, and F. Simkovic, *Phys. Rev. D* **92**, 093004 (2015).
- [3] L. Gráf, M. Lindner, and O. Scholer, *Phys. Rev. D* **106**, 035022 (2022).
- [4] M. Duerr, M. Lindner, and K. Zuber, *Phys. Rev. D* **84**, 093004 (2011).
- [5] M. Doi, T. Kotani, and E. Takasugi, *Prog. Theor. Phys. Suppl.* **83**, 1 (1985).
- [6] D. Štefánik, R. Dvornický, F. Simkovic, and P. Vogel, *Phys. Rev. C* **92**, 055502 (2015).
- [7] T. Tomoda, *Nucl. Phys. A* **484**, 635 (1988).
- [8] T. Tomoda, *Phys. Lett. B* **474**, 245 (2000).
- [9] D. L. Fang and A. Faessler, *Phys. Rev. C* **103**, 045501 (2021).
- [10] M. L. Goldberger and S. B. Treiman, *Phys. Rev.* **111**, 354 (1958).
- [11] V. Cirigliano, W. Dekens, J. de Vries, M. L. Graesser, and E. Mereghetti, *J. High Energy Phys.* **12** (2017) 082.
- [12] E. Caurier, F. Nowacki, A. Poves, and J. Retamosa, *Nucl. Phys. A* **654**, 973c (1999); J. Menendez, A. Poves, E. Caurier, and F. Nowacki, *ibid.* **818**, 139 (2009); E. Caurier, F. Nowacki, and A. Poves, *Phys. Lett. B* **711**, 62 (2012).
- [13] J. Menéndez, *J. Phys. G: Nucl. Part. Phys.* **45**, 014003 (2018).
- [14] J. Barea, J. Kotila, and F. Iachello, *Phys. Rev. C* **87**, 014315 (2013); **91**, 034304 (2015).
- [15] T. R. Rodríguez and G. Martínez-Pinedo, *Phys. Rev. Lett.* **105**, 252503 (2010).
- [16] L. S. Song, J. M. Yao, P. Ring, and J. Meng, *Phys. Rev. C* **90**, 054309 (2014); J. M. Yao, L. S. Song, K. Hagino, P. Ring, and J. Meng, *ibid.* **91**, 024316 (2015); L. S. Song, J. M. Yao, P. Ring, and J. Meng, *ibid.* **95**, 024305 (2017).
- [17] P. K. Rath, R. Chandra, K. Chaturvedi, P. Lohani, P. K. Raina, and J. G. Hirsch, *Phys. Rev. C* **88**, 064322 (2013).
- [18] F. Šimkovic, G. Pantis, J. D. Vergados, and A. Faessler, *Phys. Rev. C* **60**, 055502 (1999).
- [19] F. Šimkovic, V. Rodin, A. Faessler, and P. Vogel, *Phys. Rev. C* **87**, 045501 (2013).
- [20] J. Hyvärinen and J. Suhonen, *Phys. Rev. C* **91**, 024613 (2015).
- [21] D. L. Fang, A. Faessler, and F. Simkovic, *Phys. Rev. C* **97**, 045503 (2018).
- [22] J. M. Yao, J. Meng, Y. F. Niu, and P. Ring, *Prog. Part. Nucl. Phys.* **126**, 103965 (2022).
- [23] M. Agostini, G. Benato, J. A. Detwiler, J. Menéndez, and F. Vissani, *arXiv:2202.01787*.
- [24] K. Muto, E. Bender, and H. V. Klapdor, *Z. Phys. A* **334**, 187 (1989).
- [25] F. Šimkovic, D. Štefánik, and R. Dvornický, *Front. Phys.* **5**, 57 (2017).
- [26] M. Horoi and A. Neacsu, *Phys. Rev. D* **93**, 113014 (2016).
- [27] M. Horoi and A. Neacsu, *Phys. Rev. C* **98**, 035502 (2018).
- [28] F. Ahmed and M. Horoi, *Phys. Rev. C* **101**, 035504 (2020).
- [29] S. Sarkar, Y. Iwata, and P. K. Raina, *Phys. Rev. C* **102**, 034317 (2020).
- [30] Y. Iwata and S. Sarkar, *Front. Astron. Space Sci.* **8**, 727880 (2021).
- [31] P. K. Rath, R. Chandra, K. Chaturvedi, and P. K. Raina, *Front. Phys.* **7**, 64 (2019).
- [32] E. Caurier, F. Nowacki, A. Poves, and J. Retamosa, *Phys. Rev. Lett.* **77**, 1954 (1996).
- [33] V. Cirigliano, W. Dekens, J. de Vries, M. L. Graesser, and E. Mereghetti, *J. High Energy Phys.* **12** (2018) 097.
- [34] J. Kotila and F. Iachello, *Phys. Rev. C* **85**, 034316 (2012).
- [35] J. Suhonen and O. Civitarese, *Phys. Lett. B* **308**, 212 (1993).
- [36] D. L. Fang and A. Faessler, *Chin. Phys. C* **44**, 084104 (2020).
- [37] F. Salvat, J. Fernandez-Varea, and W. Williamson, Jr., *Comput. Phys. Commun.* **90**, 151 (1995).
- [38] I. J. Arnuquist *et al.* (MAJORANA Collaboration), *Phys. Rev. C* **103**, 015501 (2021).
- [39] A. S. Barabash, *AIP Conf. Proc.* **1894**, 020002 (2017).
- [40] F. Šimkovic, A. Faessler, H. Muther, V. Rodin, and M. Stauf, *Phys. Rev. C* **79**, 055501 (2009).